Marginally stable recent Plinian eruptions of Mt. Pelée volcano (Lesser Antilles): the P2 AD 280 eruption

Guillaume Carazzo, Stephen Tait, Edouard Kaminski

Marginally stable recent Plinian eruptions of Mt. Pelée volcano (Lesser Antilles): The P2 AD 280 eruption

Guillaume Carazzo[1,2], Stephen Tait[2], and Edouard Kaminski[2]

[1]Observatoire Volcanologique et Sismologique de Martinique, Institut de Physique du Globe de Paris, Sorbonne Paris Cité, CNRS, Morne des Cadets, F-97250 Fonds St Denis, Martinique, France

[2]Institut de Physique du Globe de Paris, Sorbonne Paris Cité, Université Paris Diderot, CNRS, 1 rue Jussieu, F-75005 Paris, France

Abstract

Major volcanic hazards in the Lesser Antilles arc include powerful Plinian explosive eruptions that inject ash high into the atmosphere and produce dangerous pyroclastic density currents (PDC) on the ground. Understanding the key physical processes governing the dynamics and stability of past volcanic columns is a fundamental problem in volcanology as well as being central to assessing specific hazards in this region and elsewhere. However, the number of cases for which the transition of regime between a stable and collapsing eruptive plume is described in detail remains too small to constrain fully theoretical models of volcanic plumes. Here we present a detailed reconstruction of the time evolution of the P2 AD 280 eruption at Mt Pelée volcano in Martinique, to expand the database available to test physical models. The P2 sequence, which forced the first inhabitants to flee to other islands for decades as suggested by archaeological evidence, starts with a basal ash layer interpreted as the result of an initial violent laterally directed explosion to the NE of the volcano. Most of the deposit sequence is made of a pumice fall deposit interbedded with a low-concentration PDC deposit interpreted as the result of a partial column collapse. The upper pumice fall unit shows an inverse gradation and is overlain by a final high-concentration PDC deposit or locally by the correlative low-concentration PDC deposit. Field data on deposit dispersal, thickness, and grain-size distribution are used together with physical models to reconstruct the dynamic evolution of this eruption. Empirical models of deposit thinning suggest that the minimum volume of pyroclastic deposits is 0.67-0.88 km^3 DRE, much larger than the 0.17 km^3 DRE previously estimated. We find that the mass eruption rate increased from 6×10^7 to 1.1×10^8 kg s^{-1}, producing an initially stable 23 to 26-km-high Plinian plume, which ultimately collapsed to form a fountain. We discuss the mechanisms leading to column collapse based on published data on magmatic water contents, and our estimates of grain-size distributions and mass discharge rates. The eruption started close to the plume/fountain transition and the volcanic column ultimately collapsed mainly due to an increase in mass discharge rate. This marginally stable evolution was also inferred from analysis of the P1 AD 1300 eruption deposits, suggesting consistent behavior during the recent Plinian eruptions of Mt Pelée volcano. In these two eruptions the transition occurred at conditions well predicted by our theoretical model of volcanic plumes.

Keywords

Mt Pelée volcano, Plinian eruption, tephra dispersal, column collapse, eruptive dynamics

Introduction

Mt Pelée volcano is located in the central part of the Lesser Antilles Arc on Martinique Island. It has been the only active volcano on the island for the last 127 ky (Germa et al., 2015). Field studies of past eruption deposits show that this volcano has produced numerous dome-forming (Pelean-type) eruptions with violent explosions of the erupted dome generating pyroclastic density currents (PDCs), commonly laterally directed (e.g., 1902-1905), and open-vent pumiceous (Plinian-type) eruptions with sustained columns of gas and ash that reach several tens of kilometers in the atmosphere before collapsing and feeding PDCs channelized in the valleys (e.g., the P1 AD 1300 eruption, Carazzo et al., 2012). This succession of eruptive styles is characteristic of the stratovolcanoes in the Lesser Antilles arc as suggested by reconstructions of past eruptions from the analysis of their deposits (Roobol and Smith 1980, 2004; Boudon et al. 2005; Lindsay et al. 2005).

One important goal of physical volcanology is to identify the hierarchy of key physical processes that control the stability of explosive (or Plinian) eruption columns. As illustrated in the recent review and benchmark analysis of Costa et al. (2016), an inventory of key processes is now established, and there is some reasonable agreement between different modeling approaches. Nevertheless, some important differences remain between model predictions that stem from different hypotheses used for the theoretical description of a volcanic plume (Costa et al. 2016). A systematic confrontation of model predictions with high quality and high resolution field data is thus necessary to achieve the more enduring goal of identifying the physical processes and most appropriate theoretical framework applicable to plume evolution. In a recent theoretical study (Michaud-Dubuy et al. 2018), we showed that amongst the only two cases where the eruption conditions and the transition were well enough described to constrain our theoretical model of volcanic plumes, PPM, the ≈186 CE Taupo and 79 CE Vesuvius eruptions, only the transition for the Taupo eruption was correctly predicted by the model. In short, we do not yet have a well-populated inventory of eruptions, all characterized to the same level of detail, such that modeling studies exploring individual physical effects can be readily tested with quantitative precision. In an effort to remedy this state of affairs, we have undertaken a long-term, systematic study of the Plinian eruptions of Mt Pelée volcano as these tend to systematically produce both stable plumes and collapsing fountains (Traineau et al. 1989). The P2 eruption, the focus of the current paper, sits notably in the middle of a sequence of three explosive events, all broadly similar in terms of magma composition and volume, spanning the relatively short interval of ≈1300 years, implying that they all came from the same storage zone. The recent Plinian eruptions of Mt Pelée volcano therefore provide a special opportunity to look carefully through the lens of a physical model at the processes affecting column stability in a context of several events which have much in common.

We build upon previous studies of the last Plinian eruption on Martinique, which is named P1 and dated at AD 1300 ± 20 from ^{14}C measurements on charcoal (Westercamp and Traineau 1983; Traineau et al. 1989). After an initial dome-forming (Pelean-type) stage (Villemant and Boudon 1999), a 19 to 22 km-high Plinian column rose in the atmosphere and spread volcanic ash to the SW direction before partially, and then totally collapsing to form a 1.3 km-high fountain feeding PDCs (Carazzo et al. 2012). The transition from a sustained column to a collapsing fountain commonly occurs when the eruption intensity increases and/or when the amount of exsolved gas at the vent decreases (Wilson et al. 1980; Carey and Sigurdsson 1989; Valentine and Wohletz 1989; Neri and Dobran 1994; Suzuki et al. 2005; Carazzo et al. 2008a). The Plinian phase of the P1 eruption underwent, however, the competing effects of the stabilizing increase in effective gas content and the destabilizing increase in mass discharge rate (Carazzo et al., 2012). Two other young Plinian deposits, P3

(2010 ± 140 BP) and P2 (1670 ± 40 BP), can be used to reconstruct the recent eruptive sequences of Mt Pelée volcano and to ask whether the P1 behavior is systematic of Mt Pelée volcano eruptions. Because these three eruptions hold much in common they can provide a stringent test of the performance of our physical model. In particular, as their source conditions are identical, they can be helpful to decipher the role of total grain-size distribution which is involved in the release of gas at fragmentation, the change of mass load in the column by sedimentation, and the change of buoyancy as a function of thermal disequilibrium between gas and pyroclasts (e.g., Woods and Bursik 1991; Girault et al 2016; Michaud-Dubuy et al. 2018).

The P2 and P3 eruptive sequences are described in the literature (Roobol and Smith 1976; Westercamp and Traineau 1983; Traineau et al. 1989). However, our reinterpretation of some of the P2 deposits to the east and northeast of the volcano, which were considered to be P1 deposits by Traineau et al (1989), led to important changes in the previously estimated eruptive parameters for the P1 eruption (Carazzo et al. 2012) and necessitates a reanalysis of the P2 deposits. This paper addresses that issue by reconstructing a detailed time evolution of the eruptive parameters of the penultimate Plinian eruption of Mt Pelée volcano based on a new comprehensive field study. We use physical models and field data to estimate crucial eruptive parameters that are currently unknown (column height and mass discharge rate) and to discuss the mechanisms controlling the dynamics of this Plinian eruption.

Mt Pelée volcano

Recent eruptive history

Mt Pelée experienced four constructional stages and three destructional events (Boudon et al. 2013; Germa et al. 2015). The first stage (550-127 ky) is characterized by construction of a primitive cone and by effusive eruptions of Mt Conil located to the NE of the present cone. Sedimentological analyses of the eruptive products suggest that lavas initially erupted from several submarine vents (Vincent et al. 1989) before being erupted through a central vent above sea level (Germa et al. 2011). A voluminous flank collapse of 25 km^3 (the Le Prêcheur event) at 127 ka destroyed the southern flank of Mt Conil (Le Friant et al. 2003; Boudon et al. 2005; Brunet et al. 2016). The second building stage (127-25 ky) corresponds to the growth of a paleo-Pelée in the structure resulting from the flank collapse and ends with a second flank collapse (the St. Pierre event) that produced a 13-km^3 debris avalanche into the Caribbean Sea. The third stage of construction, named the St Vincent period, corresponds to a succession of scoria flows (Traineau et al. 1983; Bourdier et al. 1985; Boudon 1993). Two major eruptions occurred during this period of high magma production (SV1 and SV2) producing more than 1 km^3 of magma each (Traineau et al. 1983). After a period of quiescence, a third flank collapse occurred at 9 ka (the Rivière Sèche event) producing a 2-km^3 debris avalanche (Le Friant et al. 2003). The last building stage (9 ky to present) corresponds to the neo-Pelée period with a succession of Pelean and Plinian eruptions (Roobol and Smith 1976; Westercamp and Traineau 1983).

The recent eruptive history of Mt Pelée is well documented through several field-based studies (Roobol and Smith 1976, 1980; Fisher et al. 1980; Westercamp and Traineau 1983; Bardintzeff et al. 1989; Boudon and Lajoie 1989; Bourdier et al. 1989; Lajoie et al. 1989; Traineau et al. 1989; Boudon et al. 2005; Carazzo et al. 2012; Wright et al. 2016), petro-geochemical analyses (Dupuy et al. 1985; Quantin et al. 1991; Villemant et al. 1996; Martel et al. 1998, 2000; Villemant and Boudon 1998, 1999; Martel and Poussineau 2007; Ruzié and Moreira 2010; Davidson and Wilson 2012; Martel 2012), and palaeomagnetic measurements (Genevey et al. 2002; Bernard et al. 2007). Measurements of ^{14}C on samples

collected on land indicate that at least 28 magmatic eruptions occurred during the last 16,000 years (Westercamp and Traineau 1983; Boudon et al. 2005). Tephrochronological studies on deep-sea sediment cores suggest that this number may be considerably underestimated (Boudon et al. 2013). Archaeological artefacts found at the base of pumice fall deposits indicate that Pre-Columbian peoples witnessed the three most recent Plinian eruptions of Mt Pelée volcano (Bérard et al. 2001; Saunders 2005), namely P3, P2 and P1. Historical documents also report two minor phreatic eruptions in 1792 and 1851 (Perrey 1853), and two dome-forming (Pelean) eruptions in 1902-1905 (Lacroix 1904) and 1929-1932 (Arsandaux 1929, 1934; Perret 1931a,b, 1935; Revert 1931; Romer 1931, 1934).

Overview of the P2 Plinian eruption

The P2 Plinian eruption is dated at AD 280 ± 40 based on the average of six ^{14}C ages (Westercamp and Traineau 1983). The opening phase of this magmatic event produced a laterally directed blast disrupting the settlement of Saladoid people on the Northeastern coast of Martinique (Bérard et al. 2001). Immediately after this violent explosion, a Plinian column formed covering the northeastern slopes of the volcano with pumice fall deposits (Fig. 1a). The final sequence of P2 corresponds to dense PDCs in several valleys to the east and southwest and/or to the correlative dilute PDC deposits (Fig. 1b). Volume estimates for the Plinian fall deposits yield 0.17 km^3 DRE (Traineau et al. 1989) but the field data collected were too scarce to calculate a maximum column height. Previous petro-geochemical measurements provide quantitative estimates of pre-eruptive magma storage conditions, including temperature (1,150 K), fragmentation pressure (40-70 MPa), and post-eruptive water content from measurements in interstitial glasses (2.5 ± 0.3 wt.%) (Martel and Poussineau 2007).

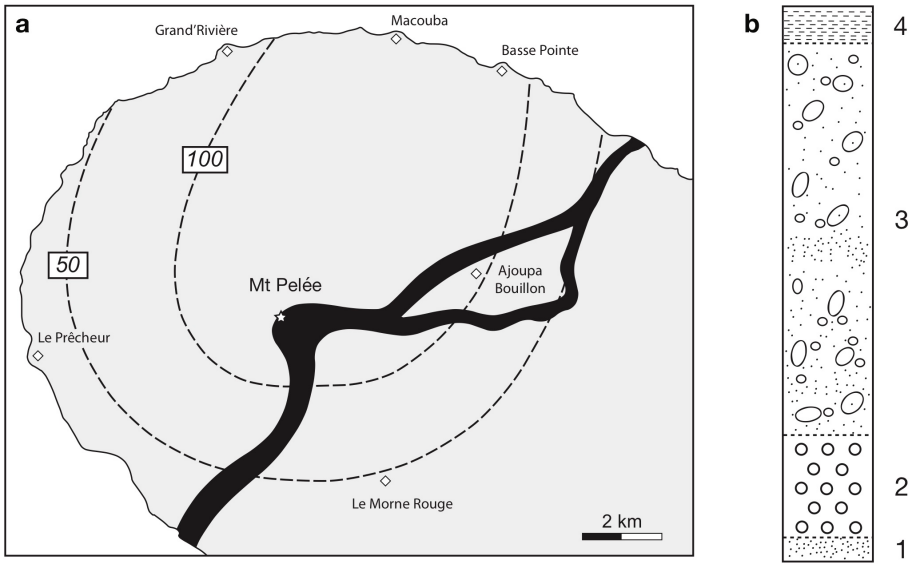

Fig. 1: **a** Isopach map (in centimeters) and **b** composite stratigraphic log of the P2 sequence proposed by Traineau et al. (1989) (1: fine grey lithic ash fall deposit; 2: Plinian fall deposit; 3: PDC deposit; 4: fine ash deposit). Open diamonds give the location of the main towns.

Stratigraphy of the P2 eruption

We have identified P2 eruption deposits at more than 80 locations on Martinique Island during extensive fieldwork (Fig. 2). Most of the studied outcrops are located from north to east of the vent. Exposure is very limited to the northwest where dense tropical forest grows

on the steep slopes of Mt Conil and other volcanic hills making it very difficult to explore this region. Based on diagnostic sedimentary, stratigraphic and physical features of the deposits, we divide the P2 eruption into five major phases characterized by specific deposits.

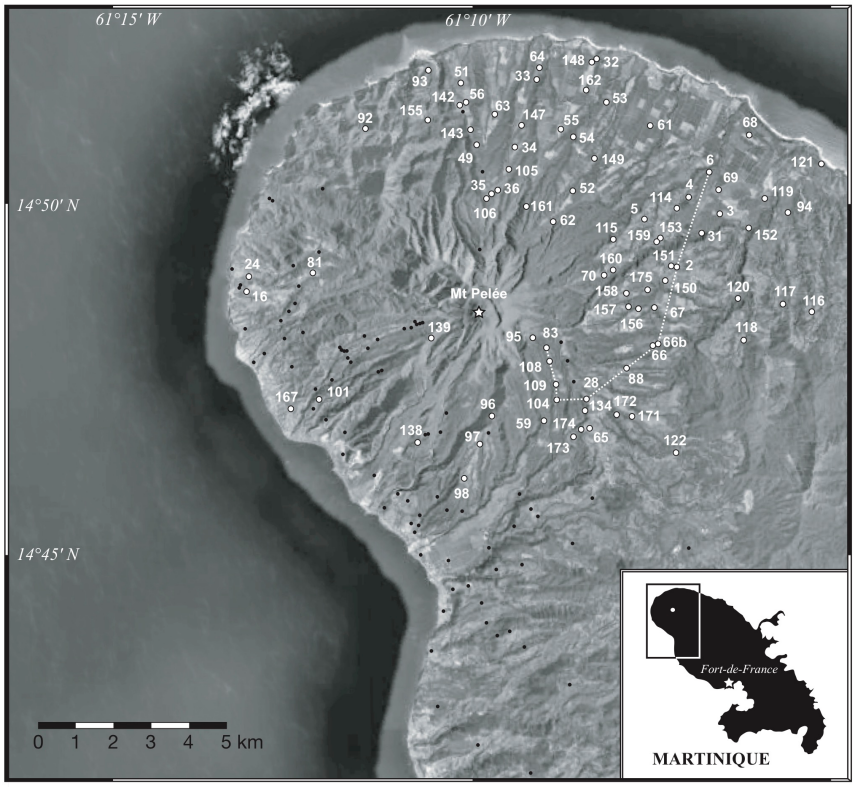

Fig. 2: Overview of Martinique (inset). White circles and numbers refer to localities where P2 deposits are present. Black dots show outcrop location where P2 is absent (due to erosion and/or too deeply buried under recent eruption deposits). The dotted line gives the stratigraphic correlation reported in Fig. 6

Phase P2i

The eruption started with the emplacement of a thin (2-7 cm) dark grey lithic-rich fine ash layer over 75 km^2 to the northeast of the vent during an opening phase. This ash layer is stratified, unconsolidated and rich in accidental lapilli-size lithic fragments at proximal locations. At many sites, the contact with the overlying layer is sharp, without an erosional surface (Fig. 3a-c, g).

Unit P2i varies irregularly in thickness with distance from the source ranging from 5 to 20 cm at 3.2 km from the eruptive center (Fig. 3a). It is absent on the west and south flanks of the volcano but can be found up to 7.5 km in the northeast direction. The relative widespread dispersion in a single direction, its irregular thickness, framework (matrix-supported), and grain-size types (juvenile and accidental lithic materials) indicate that unit P2i is a low-concentration pyroclastic density current deposit emplaced from a violent lateral blast directed to the northeast. The P2i unit covers some archaeological ceramic artefacts from the ancient Saladoid period (AD 0 to 300) suggesting that the blast reached and destroyed several settlements on the Atlantic coast (Bérard et al. 2001).

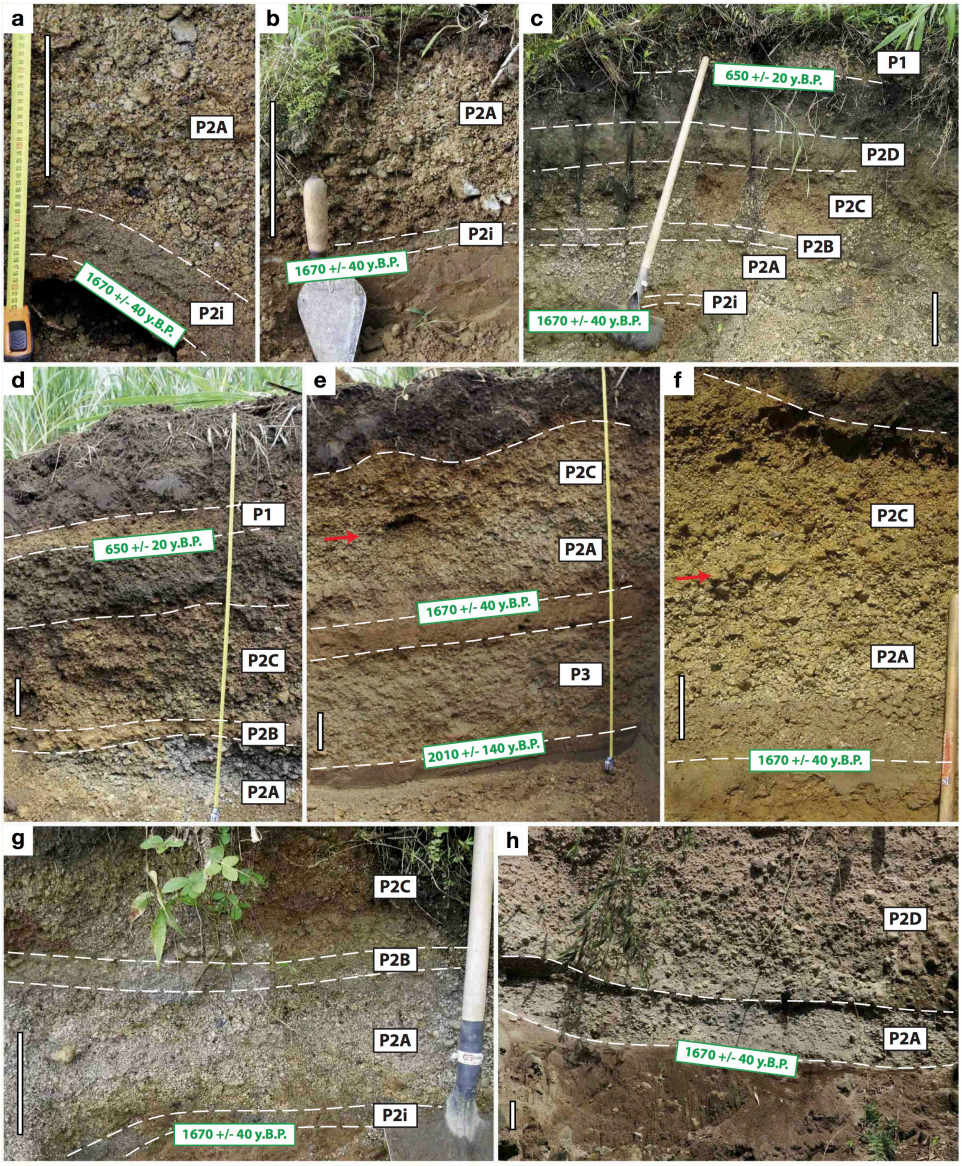

Fig. 3: Representative photographs of outcrops of the P2 deposits in Martinique at sites **a** 115, **b** 157, **c** 109, **d** 143, **e** 142, **f** 56, **g** 108, and **h** 152. See Fig. 2 for location and distance from the source. All scale bars are 20 cm long

Phase P2A

The main layer of the P2 sequence (P2A) is a blanket of clast-supported, white pumice lapilli although, a few grey pumices are present, (Fig. 3a-h) bearing juvenile and accidental lithic fragments in a total amount that typically increases from 2 wt.% at base to 6 wt.% at top. At most sites, both pumice and maximum lithic size increase slightly in the uppermost part of the unit.

In the downwind direction to the northeast, unit P2A has a maximum thickness of 280 cm at 3.2 km from the crater, steadily thinning to 50 cm within 7.5 km of the crater. In the crosswind direction, unit P2A is 60 cm thick in the most proximal sections, thinning to 25 cm within 4.2 km of the crater. The relatively widespread nature of this deposit, its uniformly decreasing thickness with distance from the source, framework (clast-supported), and grain types (pumice and juvenile lithic fragments) characteristics indicate that unit P2A is a fall deposit.

Phase P2B

P2B is a unit of brown ash-grade material in which lithic fragments and crystals are dispersed in a matrix of dense, angular, glass fragments. All materials range from fine to coarse ash. At many proximal sites, the contact with the overlying layer is sharp. On the other hand, some erosion of unit P2A locally characterizes the lower contact.

Unit P2B varies irregularly in thickness with distance from the source ranging from 5 to 35 cm at 2.6 km from the eruptive center (Fig. 3c, d, g). This unit is, however, absent beyond 6.5 km from the crater. The relatively limited dispersal of this unit, its irregular thickness, framework (matrix-supported) and grain types (juvenile and accidental lithic fragments), as well as the nature of the lower and upper contacts, indicate that unit P2B is a low-concentration pyroclastic density current deposit.

Phase P2C

Unit P2C consists of a blanket of clast-supported, white pumice lapilli (Fig. 3c-g). Juvenile lithic fragments are present with a typical content of 9 wt.%. At most sites, pumice and maximum lithic sizes, and lithic content increase from base to top. This inverse grading is pronounced in the lower 10 cm of the deposit with pumice sizes increasing from fine to coarse lapilli and juvenile lithic content increasing from 6 to 9 wt.%. The uppermost part of this deposit is often missing due to erosion in particular by intense tropical weathering and current extensive farming in banana plantations.

Unit P2C has a maximum thickness of 300 cm at 3.5 km from the crater in the downwind direction, which steadily thins down to 50 cm within 6.5 km of the crater. In the crosswind direction, unit P2C is 150 cm thick in the most proximal sections, thinning to 30 cm within 5.8 km from the eruptive center. The relatively widespread nature of this deposit, its uniformly decreasing thickness with distance from the source, its framework (clast-supported), fabric (inverse grading), and grain types (pumice and juvenile lithic materials) characteristics indicate that unit P2C is a fall deposit.

Phase P2D

Unit P2D lies uppermost in the P2 sequence and exhibits two facies. At several sites, P2D is a very poorly sorted layer of white, rounded pumice lapilli and blocks floating in a matrix of white fine ash (Fig. 3h). At other sites, the P2D unit consists of fine ash, crystals, juvenile and accidental lithic fragments with a thickness of 50 cm at 4.7 km from the volcano. The very poorly sorted nature of this deposit, the mostly valley-confined geometry and the erosion of the underlying pumice fall unit indicate that P2D is a pyroclastic density current deposit. The high-concentration deposits can be found in valleys whereas low-concentration deposits, most likely related to a detaching dilute PDC from the top of the main flow, can be found on hills.

Grain-size analyses

Methods

The P2 eruption deposits were sampled for sieving analysis, and the samples dried for 24 h in an oven and sieved by hand down to 6ϕ. A binocular microscope was used to discard crystals and lithic fragments in the size range −4ϕ to −2ϕ. The cumulative frequency curves were determined using the method of Kaminski and Jaupart (1998), which accounts for the power law size distribution of the rock fragments (Hartmann 1969; Turcotte 1986; Alibidirov and

Dingwell 1996; Kueppers et al. 2006):

$$N(R_p \geq r_p) = \lambda r^{-D}, \quad (1)$$

where $N(R_p \geq r_p)$ is the number of particles with a radius larger than r, and D is the power-law exponent. The latter fully characterizes the grain-size distribution and is found to vary between 2.9 and 3.9 for Plinian eruptions (Kaminski and Jaupart 1998; Girault et al. 2014).

The total grain-size distribution of an explosive eruption is not straightforward to determine because (i) coarse-grained particles are often very brittle and break up during sampling, (ii) fine-grained particles are transported over large distances from the vent and are not taken into account in the estimations, and (iii) significant uncertainties in sieving analyses may arise for medium coarse-grained particles (Koyaguchi and Ohno 2001). However, because fragmentation is a size-invariant process (Turcotte 1986), the coefficient D can be estimated accurately using any sufficiently large range of sizes. Thus, only data at lapilli size can be used and the lack of fine-grained particles lost out at sea does not affect the estimation of D.

Grain-size distributions of selected representative samples

Grain-size analyses were carried out for representative samples of the different eruptive units from selected locations (Table 1). The P2i unit is fine grained and poorly sorted with a relatively broad unimodal distribution (Fig. 4a). The median diameter (Md -0.4 to 0.4 ϕ) and sorting (σ 1.6 to 2.2) have the values typical of surge deposits and the amounts of ash (< 2 mm) reach up to 80-93 wt. %.

Sample	Site	Unit	Subunit	Altitude (m)	Distance from the vent (km)	Thickness (cm)
1	95	P2A	Bulk	865	1.6	50
2	157	P2i	Bulk	433	3.9	4
3	88	P2A	Bulk	466	4.3	70
4	115	P2i	Bulk	304	4.3	5
5	34	P2B	Bulk	313	4.9	7
6	34	P2C	Base	313	4.9	115
7	34	P2C	Top	313	4.9	115
8	66b	P2A	Bulk	371	4.9	85
9	54	P2A	Base	203	5.6	140
10	142	P2A	Base	234	5.8	65
11	142	P2A	Top	234	5.8	65
12	142	P2C	Bulk	234	5.8	32
13	194	P2i	Bulk	280	5.9	3
14	194	P2A-C	Bulk	280	5.9	70
15	114	P2A-C	Bulk	195	6.3	60
16	33	P2C	Base	137	6.8	32
17	64	P2A	Bulk	102	7.0	65
18	120	P2A-C	bulk	184	7.1	55
19	6	P2i	Bulk	110	7.4	2
20	119	P2i	Bulk	65	8.4	1

Table 1: Sampling of the P2 deposits for grain-size analysis.

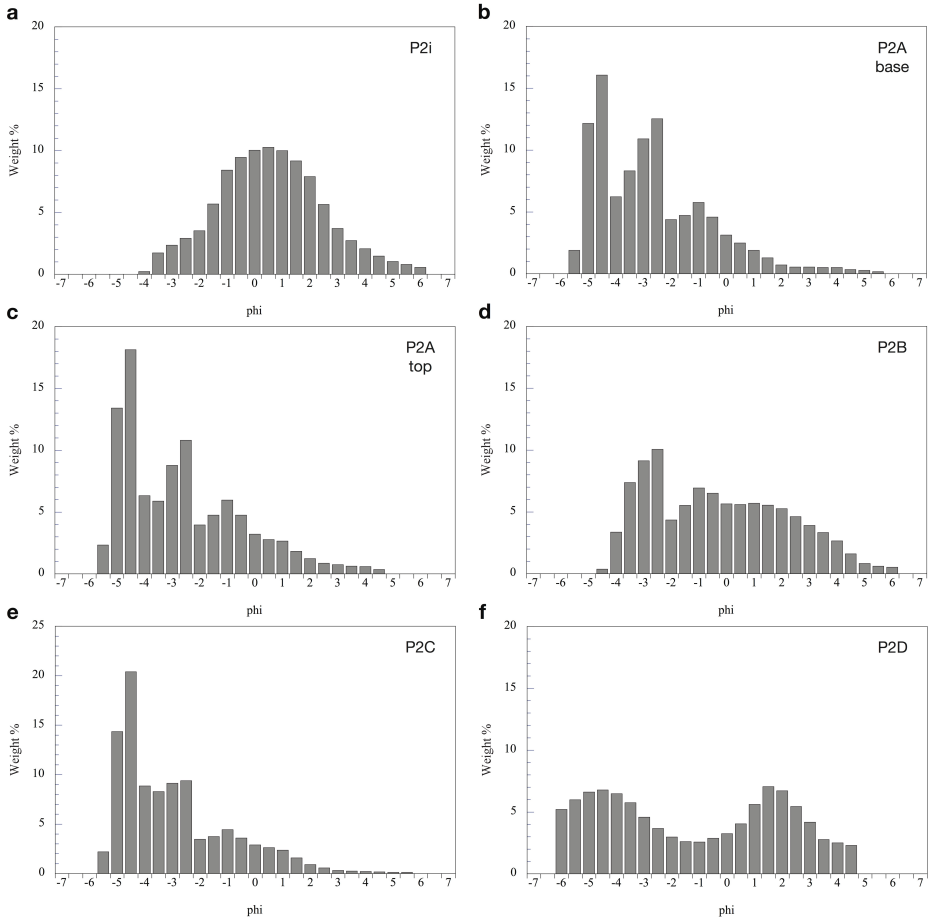

Fig. 4: Grain-size distribution of selected samples representing the **a** P2i, **b** P2A at base, **c** P2A at top, **d** P2B, **e** P2C, and **f** P2D units

The P2A unit shows typical fallout characteristics with median diameter ranging from -4.3 to -2 ϕ and sorting (σ) ranging from 1.1 to 2.2. These values are consistent with those of Bardintzeff et al (1989) who measured Md ranging from -3.6 to -0.9 ϕ and sorting ranging from 1.1 to 2.9. The grain-size analyses performed on the P2 deposits mostly include proximal samples because medial and distal deposits were lost at sea. The grain-size distribution of individual samples is generally bimodal with variations in minimum, maximum, and modal grain-size depending on the distance from the vent and wind direction. The top of the P2A unit (Fig. 4b) is always slightly coarser grained than the base (Fig. 4c) but the sorting and amounts of ash (< 2 mm) remain approximately constant throughout the unit (i.e. between 20 and 45 wt. % depending on outcrop location).

Unit P2B is more poorly sorted than unit P2A, and has both fall and flow features. The bimodal sample in Fig. 4d has a relatively broad distribution with two marked populations: a primary coarser mode at -3 to -2 ϕ and a secondary finer mode at -1.5 to -0.5 ϕ. The amount of ash is much larger than in unit P2A (i.e., 57 wt. %).

The P2C unit has characteristics similar to the P2A unit (Fig. 4e) with median diameter ranging from -4 to -2.4 ϕ and sorting ranging from 1.6 to 1.9. The grain-size distribution of individual samples is also bimodal with peaks at -4.5 and -2.5 ϕ similarly to the P2A unit. The amounts of ash (< 2 mm) are however slightly larger than in the P2A unit (i.e., between 20 and 40 wt. % depending on outcrop location).

Unit P2D shows a relatively broad distribution with bimodal populations (Fig. 4f). This deposit is a combination of a coarser population in the pumice clasts with primary mode

at -5 to -4 ϕ, and a finer population in the isolated crystals with secondary mode at 1.5 to 2 ϕ. The sorting exhibits features typical of flows with values up to 3.6.

Total grain-size distributions

The total grain-size distributions of the P2A and P2C units are calculated using the method of Kaminski and Jaupart (1998). We evaluated the total mass in sieve class ϕ, M_ϕ, by the volume integral

$$M_\phi = \int_0^L h(l)\, C_\phi(l)\, A(l)\, dl, \qquad (2)$$

where $h(l)$ is the deposit thickness, $C_\phi(l)$ is the concentration of class ϕ at distance l from the vent, $A(l)dl$ is the area bounded by isopachs at distances l and l+dl, and L is the distance where h or C_ϕ drop to zero. We used linear interpolations for h and C_ϕ between the localities. The total grain-size distributions of both units are bimodal with a primary mode at -3.5 to -2.5 ϕ and a secondary mode at -1 to -0.5 ϕ for both units (Fig. 5). The median diameter is -3.1 ϕ for P2A and -2.8 ϕ for P2C, and the sorting is 2 for P2A and 1.8 for P2C. The ash fraction (< 2 mm) reaches 29 wt.% for P2A and 33 wt. % for P2C, and the fine ash fraction (< 63 μm) accounts for only 1 wt. % in both units. The latter value is certainly underestimated since most of the fine ash settled at sea and cannot be taken into account in our grain-size analyses. From these results, we infer that the power law coefficient D = 3.5 ± 0.1 during the P2A phase and D = 3.4 ± 0.1 during the P2C phase (Fig. 5).

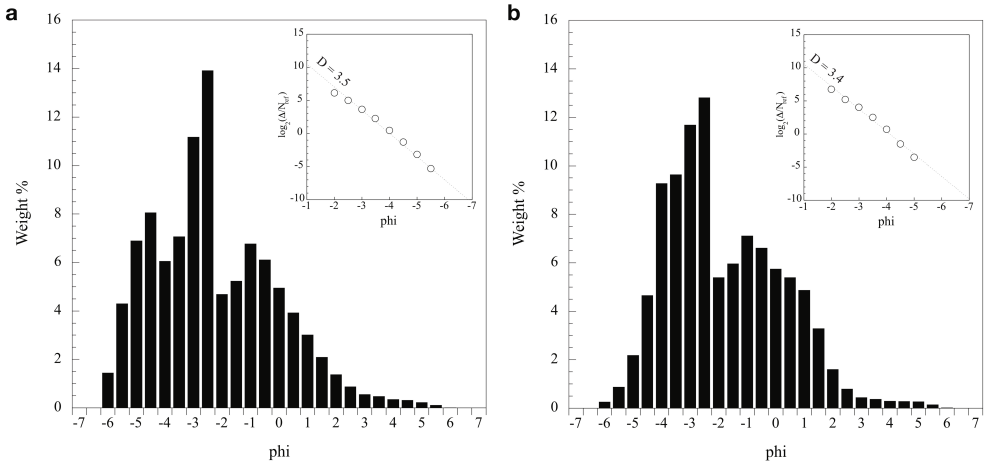

Fig. 5: Reconstructed total grain-size distribution for **a** the P2A and **b** the P2C units. The insets show the same grain-size distributions reported as the number of fragments in each sieve class Δ normalized by an arbitrary constant N_{ref}, as a function of size. The size bounds used to estimate the power law exponent D is -2 to -6ϕ, as in Carazzo et al. (2012)

Spatial distribution of the P2 deposits

Isopach maps

Fig. 6 shows a stratigraphic correlation of P2 outcrops along two different dispersal axes. The complete sequence can be found up to 7 km from the crater (sites 83, 108, 109 and 104 in Fig. 6).

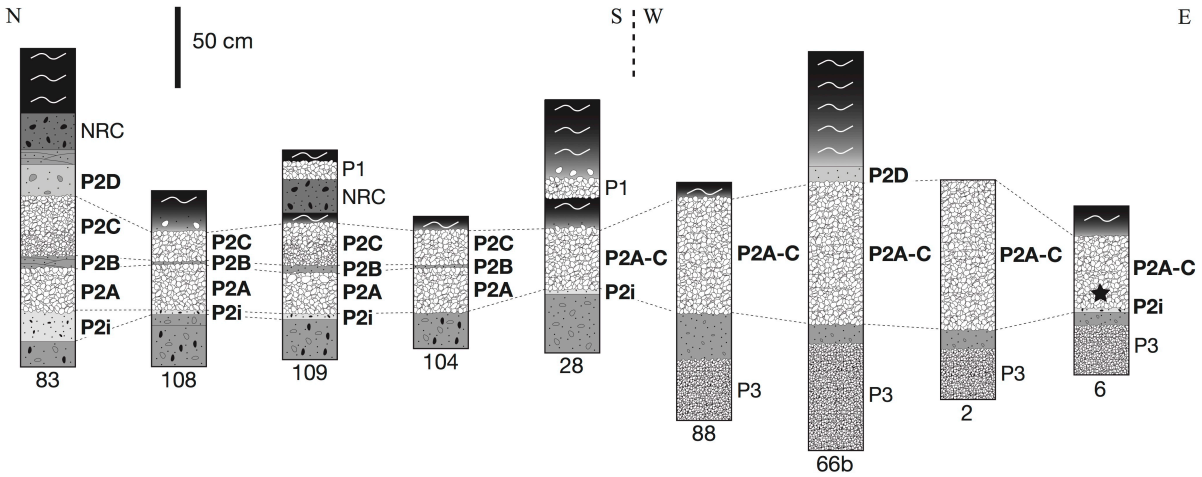

Fig. 6: Stratigraphic logs of representative sections of deposits of the P2 eruption. See Fig. 2 for location of outcrops. Log 83 is the type section displaying all the P2 units. The star gives the location of the charcoal sampled for ^{14}C dating

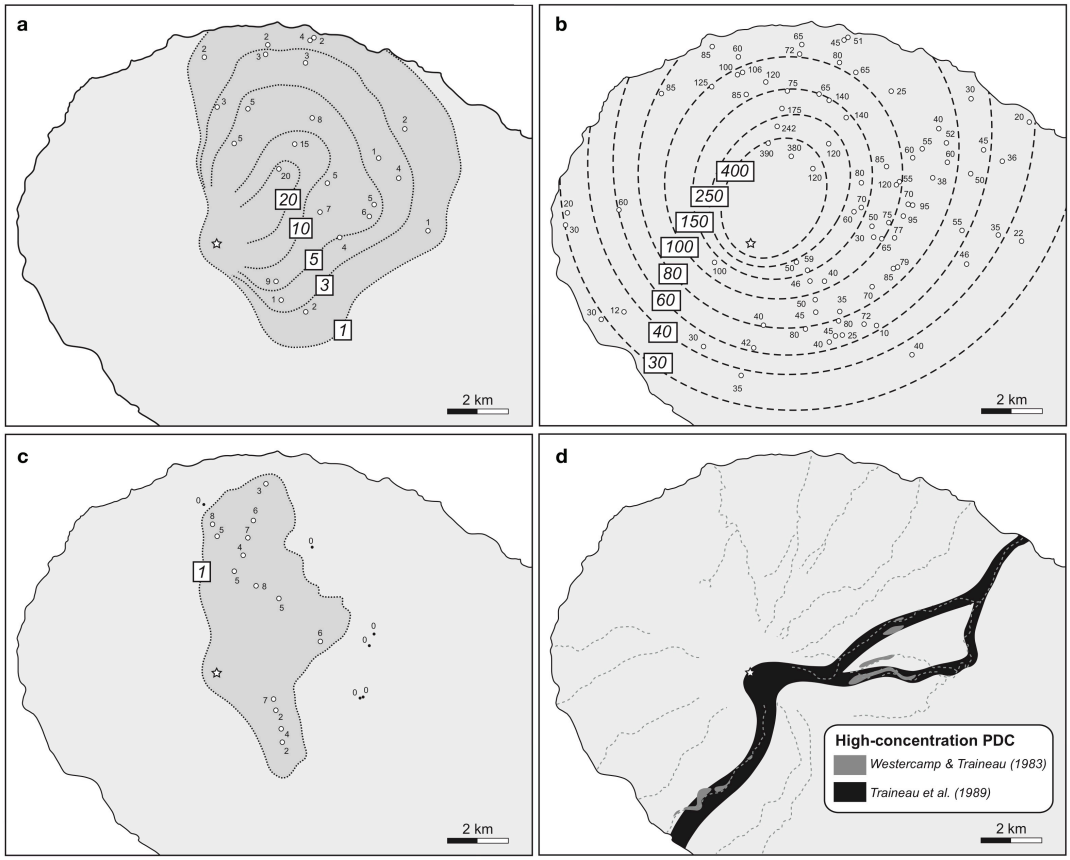

Fig. 7: Isopach maps (in centimeters) for **a** P2i, **b** the cumulative pumice fallout (P2A+P2C) from P2, **c** P2B and **d** P2D. Open circles indicate measured sample locations. Where unit P2B is missing, a fine-grained limit is observed between P2A and P2C

P2i deposits are widespread on the northeastern flank of the volcano, and vary in thickness between 20 cm at 3.2 km from the crater to 2 cm near the coasts (Fig. 7a). P2B deposits are widespread on the north and northeast flanks of the volcano but are absent beyond 6.5 km from the crater (Fig. 7c). The high-concentration PDC deposits of P2D are mainly channelized in the river valleys Sèche, Falaise, Ravine, Noire, and Capot (Fig. 7d), as described in previous studies (Westercamp and Traineau 1983; Traineau et al. 1989).

The cumulative thickness of pumice fallouts P2A and P2C is reported in a single isopach map (Fig. 7b), which shows ellipsoidal contour patterns indicating strong fallout dispersion towards the NNE. The dispersal direction is found to be in good agreement with the results of Traineau et al. (1989), which is characteristic of the wind profiles in the Lesser Antilles (Komorowski et al. 2008). The northwestern arms of our isopach map are not well constrained due to a lack of outcrop in a region extremely difficult to access due to the presence of dense tropical forest on steep hills. No previous studies have found outcrop in this area.

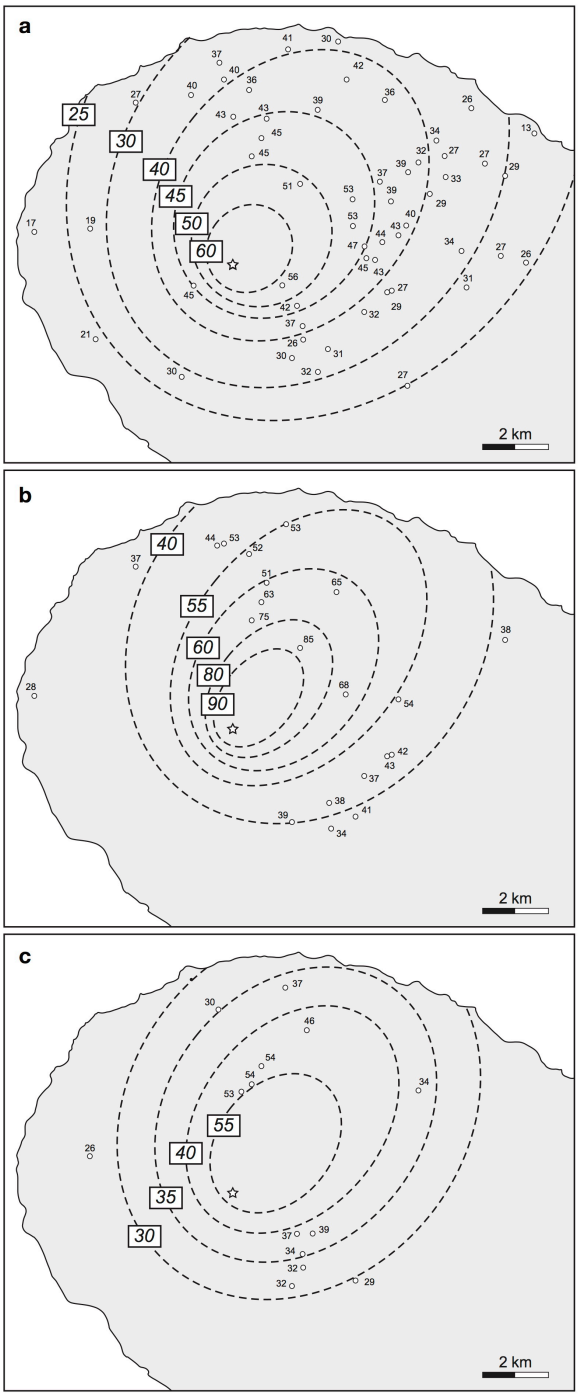

Fig. 8: Isopleth maps (in millimeters) for the lithic fragments sampled at the base and the top of P2A and the base of P2C. Open circles indicate measured sample locations. Direction of dispersal axes is consistent with those inferred from the isopach map for P2A-C

Isopleth maps of air fall deposits

Maximum lithic isopleth maps of P2A and P2C were constructed from the major axes of the five largest lithic fragments found at the base and the top of P2A and at the base of P2C (Fig. 8). The isopleth map of the base of P2A is well constrained due to the good preservation of the deposit. However, isopleth contours of the top of P2A and the base of P2C are constrained by only a few points from localities where the deposits shows a clear separation between the two pumice fallout units, such as variation in pumice size and/or the presence of the P2B unit. An isopleth map of the top of P2C could not be constructed due to erosion of P2C by intense farming in banana plantations above it. The greater extension of the top of P2A isopleth contours suggests however that the plume height and thus the mass discharge rate increased during the transition from P2A to P2B.

Eruptive dynamics

Erupted volumes

The volume of tephra fallout produced during an explosive eruption can be inferred using several methods based on the thinning trend of the deposit with distance from the source (Pyle 1989, 1995; Fierstein and Nathenson 1992; Bonadonna and Houghton 2005; Bonadonna and Costa 2012). However, because only proximal and furthermore incompletely preserved deposits are available in Martinique, volume calculations are bound to provide minimum estimates only.

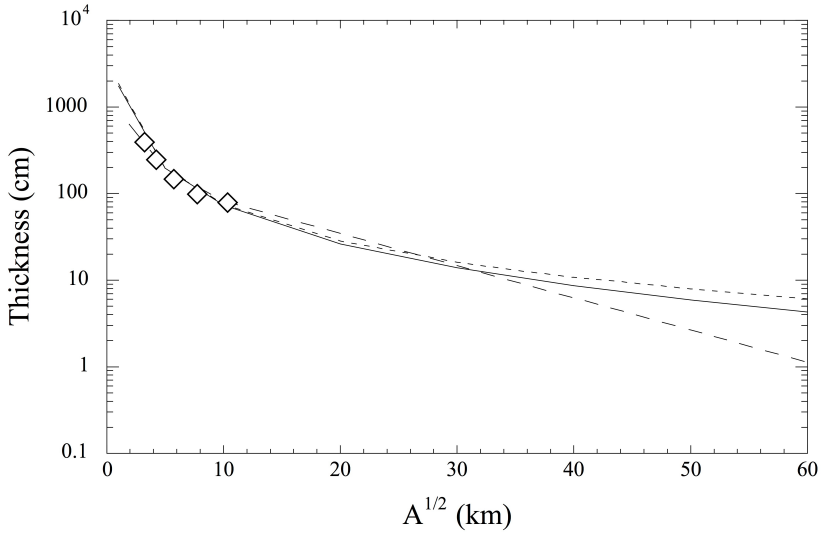

Fig. 9: Deposit thinning profiles generated from the isopach map for the cumulative pumice falls P2A+P2C. Semi-log thickness-square root of isopach area plot. Thinning trends are approximated by exponential (dashed line), power-law (dotted line) and Weibull (solid line) fits

Fig. 9 gives the thinning trend of the cumulative P2A and P2C deposits based on five proximal isopach contours since our 30 to 60 cm contours are not well constrained in the downwind direction (Fig. 7). The minimum bulk volume of P2A+P2C is calculated using a power-law, exponential and Weibull fit (Pyle 1989; Bonadonna and Houghton 2005; Bonadonna and Costa 2012) computed using the AshCalc software (Daggit et al. 2014). Integration of the two-segment exponential fit, the power-law fit, and the Weibull fit yield

volumes of 0.6, 1.8 and 1.3 km^3, respectively. Given that the exponential fit gives a minimum value because distal data is missing, we retain a bulk volume of 1.3-1.8 km^3 for the cumulative P2A and P2C fallout units. The corresponding DRE volume is 0.54-0.75 km^3 based on deposit and magma densities of 1000 and 2400 kg m^{-3}, respectively (Traineau et al., 1989).

The volume of PDC deposits is more difficult to assess. Here we use the observed relationship between the volume and area covered by dilute PDC (Dade and Huppert 1998; Calder et al. 1999), as in Carazzo et al. (2012) for the P1 eruption. Fig. 7 shows that the P2i and P2B deposits cover 70 km^2 and 30 km^2, respectively, which correspond to a bulk volume of 0.02 km^3 for P2i and 0.01 km^3 for P2B.

The total volume of the P2 eruption (P2i+P2A-C+P2B+P2D) is calculated to be 0.74 ± 0.06 km^3 DRE, which is much larger than the 0.17 km^3 DRE previously estimated (Traineau et al. 1989). We attribute this important discrepancy to (i) the large volume of PDC deposits that were not taken into account in Traineau et al. (1989), (ii) the improvement of the reconstruction techniques to calculate the total volume of a pumice fall deposit (Bonadonna and Costa 2013), and (iii) our reinterpretation of pumice fall deposits to the east and north-east of Mt Pelée volcano previously taken to be P1 rather than P2 deposits (see discussion in Carazzo et al. 2012). To reinforce our conclusion about the nature of the fallout deposits in this region, which were attributed to the P1 eruption by Traineau et al (1989), we obtained a new ^{14}C measurement on a charcoal sampled within the deposit (outcrop #6). The estimated (non-calibrated) age of this sample is 1695 ± 30 y. BP, which is consistent with the radiocarbon dates found for the P2 eruption (i.e., on average 1670 ± 40 y. BP non-calibrated ^{14}C) and confirms that our reinterpretation is correct.

The total mass of tephra emitted during the P2 eruption is estimated to be 1.5 – 1.9 x 10^{12} kg, which corresponds to a Magnitude 5.2 (Pyle 2000) and a VEI 4 event (Newhall and Self 1982).

Column heights and exit velocities (P2A and P2C)

The maximum height reached by a volcanic plume depends on a number of factors including the mass discharge rate feeding the eruption, atmospheric profiles of temperature and pressure, the amount of turbulent mixing, the grain-size distribution, and the strength and direction of atmospheric winds (Carey and Sparks 1986; Girault et al. 2016). In the Lesser Antilles, northeasterly trade and lower stratospheric winds dominate at low (< 11 km) and high (> 21 km) altitudes, whereas southwesterly antitrade winds blow at mid-altitude (11–21 km) (Traineau et al. 1989; Komorowski et al. 2008). In order to improve estimations of maximum column height in a bidirectional wind profile, we use the version of the model of Carey and Sparks (1986) adapted to the El Chichon area (Carey and Sigurdsson 1989) considering that the intensity of trade winds increases linearly from 0 to 25 m s^{-1} up to an altitude of 11 km, whereas antitrade winds blow in the opposite direction between 11 and 21 km increasing linearly up to 20 m s^{-1}. Our isopleth maps (Fig. 8) in this framework yield a maximum height of 23 ± 1 km for the beginning of P2A, 26 ± 1 km for the end of P2A, and 22 ± 1 km for the beginning of P2C. Error bars are calculated using the three values of maximum height inferred from the 8, 16, and 32-mm isopleths (see Fig. 17 in Carey and Sigurdsson 1989).

Bonadonna and Costa (2013) propose an alternative method to infer the maximum column height from variations of grain size with the distance from the source. Fig. 10 gives the decreasing trend of the maximum lithic size as a function of the square root of isopleth contours for fragments collected at the base of P2A, the top of P2A and the base of P2C. A Weibull fit can be used to determine the eruptive column height according to equation 7 of

Costa and Bonadonna (2013). Following this approach, we calculate a maximum height of 23.5 km for the beginning of P2A, 26 km for the end of P2A, and 22.5 km for the beginning of P2C. These results are remarkably close to the column heights determined with the method of Carey and Sparks (1986).

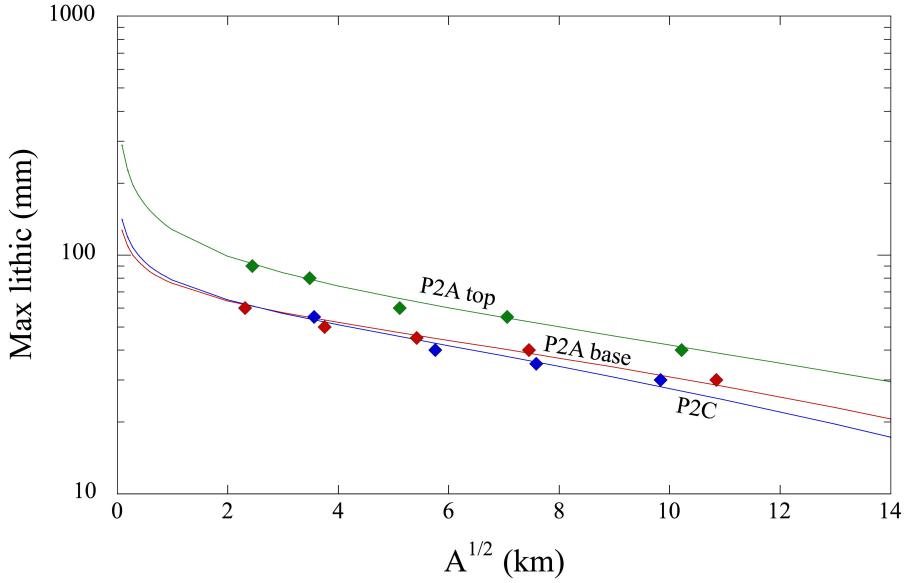

Fig. 10: Semi-log plots of square root of isopleth area (in kilometers) versus lithic clast size (in millimeters) and the Weibull best fit for the units P2A at base (red curve), P2A at top (green curve), and P2C (blue curve)

Data in Fig. 10 can also be used to estimate the vent velocity with the method of Wilson (1976). Considering the equilibrium between the upward drag and downward gravity forces for a particle just before its fall from the column edge, the momentum conservation law of the particle can be rewritten to extract the minimum velocity required at the vent to carry up the fragment. Extrapolating the curves in Fig. 10 down to $A^{1/2}$ = 0.01 km to find the maximum lithic size at the vent, we infer minimum exit velocities of 185 m s^{-1} for the beginning of P2A, 280 m s^{-1} for the end of P2A, and 195 m s^{-1} for the beginning of P2C.

Mass discharge rate and duration

The maximum mass discharge rate (MDR) feeding the eruption during P2A and P2C is inferred from a given maximum column height by using the model of Carazzo et al. (2008b). Calculations are made for tropical atmospheric conditions and for a crystal-bearing rhyolitic magma (andesitic bulk composition) with an initial temperature of 1,150 K (Martel and Poussineau 2007) and a bulk density of 2,400 kg m^{-3} (Traineau et al. 1989). The estimated values of maximum column height yield a MDR of 6±1.5 × 10^7 kg s^{-1} for the beginning of P2A, 1.1±0.1 × 10^8 kg s^{-1} for the end of P2A, and 4±1 × 10^7 kg s^{-1} for the beginning of P2C. These values correspond to an intensity of 10.6 to 11 (Pyle, 2000), and combined with the total mass of fallout deposits they provide a duration of about 7h ± 3h for the cumulative phase P2A-C, assuming no time break between the eruptive phases.

The MDR during P2B and P2D is more difficult to assess. In general, mass discharge rates are calculated from runout distances observed in the field using the model of Bursik and Woods (1996), which treats pyroclastic flows as dilute suspensions. Doyle et al. (2010) showed that this assumption is valid for tall, fine-grained column collapses, for which the flow slowly transfers its mass to the dense basal flow. We consider that the model of Bursik

and Woods (1996) is relevant for the dilute PDC of P2B, but not the dense PDC of P2D. Assuming that the dilute PDC behaved as a supercritical flow (i.e., fast (100–200 m s^{-1}) and was shallow (500– 1,000 m)) entraining air as it propagated, we find a mass flux of 2.3 ± 0.8 × 10^8 kg s^{-1}. This value does not take into account topographic slopes. Doyle et al. (2010) showed, however, that the runout distance of the upper dilute current mostly depends on the initial fountain height, which is imposed by the mass discharge rate, rather than by ground slopes. It is therefore likely that theoretical uncertainties are accounted for within the large error bars on the mass discharge rate for P2B.

Discussion

The Plinian plume / pyroclastic fountain transition

The transition from the Plinian plume to the pyroclastic fountain is strongly controlled by the mass eruption rate feeding the column and the effective exsolved gas content above the vent (Wilson et al. 1980; Valentine and Wohletz 1989; Neri and Dobran 1994; Suzuki et al. 2005; Carazzo et al. 2008a). Our estimates of the mass eruption rates show a progressive increase over time from 6±1.5 × 10^7 kg s^{-1} (P2A) to 2.3±0.8 × 10^8 kg s^{-1} (P2B). This evolution is deduced from the increase in lithic sizes in P2A and P2C and consistent with the inverse grading in pumice size in the unit P2C (see "Stratigraphy of the P2 eruption"). Other powerful eruptions underwent a similar evolution leading to the collapse of the column and the production of PDC (Walker 1980; Sigurdsson et al. 1984; Carey and Sigurdsson 1987; Sigurdsson and Carey 1989; Carey et al. 1990; Carazzo et al. 2012; Vidal et al. 2015).

The evolution of the effective gas content feeding the eruptive column is more difficult to assess. Magmatic water contents in glass inclusions have not been measured but we assume that magma storage conditions were similar before the AD 1300 P1 and the AD 280 P2 eruptions. We therefore take a total volatile content in the melt of 5.3-6.3 wt.% (Martel et al. 1998), which we correct for the presence of crystals and lithic fragments to estimate an initial gas content in the magma of 2.6-3.1 wt.%. The mass fraction of exsolved gas in the mixture at the fragmentation level is estimated to be 1.8-2.2 wt.% for a threshold vesicularity of 70 % assuming closed-system conditions. The effective amount of exsolved gas at the base of the volcanic column can differ from these values due to gas entrapment by pumices as a function of their size distribution (Kaminski and Jaupart 1998). We use the power law exponent D = 3.4-3.5 estimated in section "Grain-size analyses" to calculate an amount of 1.7-2.1 wt.% of free exsolved gas for phases P2A-C (see figure 2 of Michaud-Dubuy et al. 2018). Numerical and theoretical models simulating the decompression of a volcanic mixture show that the effective amount of free exsolved gas and the exit velocity are not independent (Woods and Bower 1995; Koyaguchi et al. 2010). Assuming that the mixture decompresses freely into the atmosphere and using equation 3.13 of Woods and Bower (1995), we calculate exit velocities after decompression in the range 180-200 m s^{-1}. These values are consistent with those estimated from the distribution of the lithic fragments at the beginning of each eruptive phase (see sub-section "Column heights and exit velocities"), which strengthens our estimates of effective gas content.

Fig. 11 compares the theoretical predictions of column collapse (Michaud-Dubuy et al. 2018) with the estimated values of mass eruptive rate and effective gas content in the column for P2. The eruptive conditions at the beginning of P2 formed a stable convective plume whose mass discharge rate increased slowly during P2A (see sub-section "Mass discharge rate and duration"). During P2A, the eruption evolved close to the plume/fountain transition, where small variations of mass flux, gas content and grain size distribution of pyroclasts have a strong impact on the flow behavior. The eruption reached a peak in mass discharge rate during P2B, which most likely induced the partial column collapse. During the final collapse

at the end of P2C, it is unclear whether the eruption reached a maximum mass discharge rate and/or a minimum in effective gas content. The increase in lithic fragment content at the top of the P2C deposits suggests that the eruption reached its maximum mass discharge rate during P2D, although no method exists to infer its exact value due to the absence of a dilute PDC deposit emplaced during this phase. The relatively good agreement between our data and the theoretical model of column collapse must be taken with caution since no accurate information exist on the evolution of the effective gas content feeding the column during the eruption. However, our results strongly suggest that the source conditions were close to the plume/fountain transition soon after the beginning of the eruption. This marginally stable evolution was also inferred from the analysis of the AD 1300 P1 eruption deposits (Fig. 11), which suggests that it could be a systematic feature of the most recent Mt Pelée volcano Plinian eruptions. In these two eruptions the transition occurred at conditions well predicted by our theoretical model of volcanic plumes (Fig. 11). Comparing these results with the ≈186 CE Taupo and 79 CE Vesuvius eruptions shows that the Taupo eruption is also correctly reproduced by the model. However, the model fails to capture the transition between the Plinian stable regime of the EU2 sequence and the collapse regime of the EU3 sequence during the Vesuvius eruption (Fig. 11). As pointed out in Michaud-Dubuy et al. (2018), the field deposits from this eruption are characterized by a specific grain-size distribution with a power-law exponent (D = 3.0) that defines the transition between a population dominated by coarser fragments (i.e., D < 3.0) and a population dominated by ash particles (i.e., D > 3.0). In fine populations (D > 3.0) dominated by ash particles the thermal coupling between the gas and pyroclasts is efficient. In coarse populations (D < 3.0), the thermal disequilibrium is large in the large fragments but those are quickly lost by sedimentation, which is the most important physical process through its effect on the mass load within the plume (Michaud-Dubuy et al. 2018). For intermediate distributions of grain-sizes (D = 3.0), pyroclasts are in average not large enough to be lost by sedimentation, but not small enough to be in thermal equilibrium with the gas. Hence, we suggest that the hypothesis of thermal equilibrium between the gas and solid phases in the column should be revisited in future models of volcanic plumes in order to explain the field data from the Vesuvius eruption.

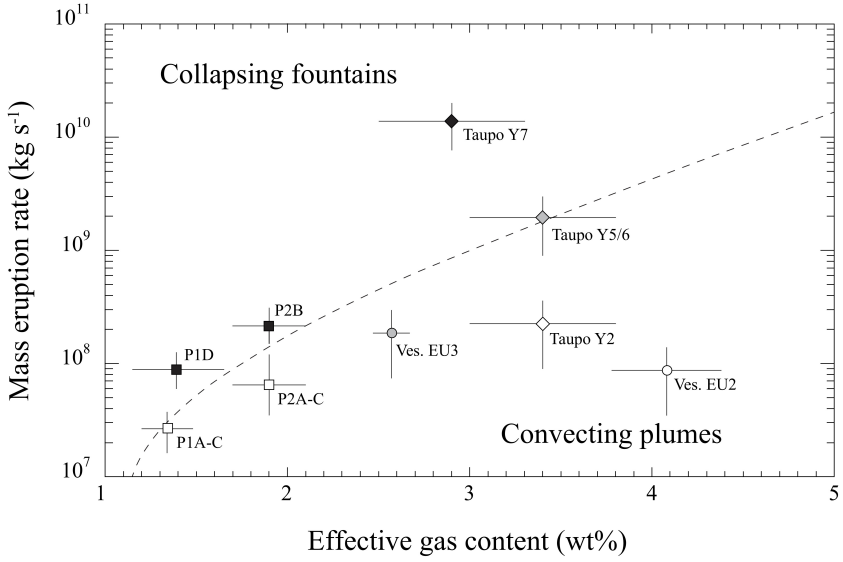

Fig. 11: Transition diagram depicting the P2 eruptive events and depositional units. Dashed line corresponds to the maximum mass eruption rate feeding a volcanic column before collapse as a function of the effective gas content at the column base (Michaud-Dubuy et al. (2018)'s model for a tropical atmosphere). Open, grey, and black symbols correspond to geological data inferred for the stable, partial and total collapse phases, respectively. Data for

the P1 eruption (squares) can be found in Carazzo et al. 2012. Data for the Taupo (diamonds) and Vesuvius (circles) eruptions are compiled in Table 1 of Michaud-Dubuy et al. (2018).

Comparison with the P1 eruption

The two latest pumice eruptions at Mt Pelée volcano (P1 and P2) have similar depositional sequences but different dispersal axes (Carazzo et al. 2012). The P1 deposits mostly settled to the southwest whereas those of the P2 eruption are found to the northeast of the volcano (Fig. 7). The volume estimated for the P2 eruption is much larger (by a factor of 5) than the one we estimated for the P1 eruption (Carazzo et al., 2012) - see Table 2. The mass eruption rates are also more powerful during the P2 eruption leading to a Plinian column with greater maximum height (22-26 km for P2 as opposed to 19-22 km for P1) and PDC with a larger run-out distance (up to 11.5 km for P2 and only 8 km for P1). The minimum eruption durations are estimated at 5h for P1 and 7h for P2 (Table 2). Grain-size analyses reveal that the eruptive products of P2 are slightly finer grained (D = 3.4-3.5) than those of P1 (D = 3.2-3.3) suggesting that magma fragmentation was more efficient during P2 and that most of the exsolved gas was free rather than being trapped in closed vesicles. Our estimates of free exsolved gas contents (1.7-2.1 wt.% for P2 and 1.2-1.5 wt.% for P1) are consistent with the minimum exit velocities inferred from the distribution of lithic fragments (180-200 m s^{-1} for P2 and 150-165 m s^{-1} for P1). Overall, as summarized in Table 2, the eruptive parameters of the P2 event correspond to a moderate Plinian eruption slightly more powerful than the P1 eruption.

Parameters	**P2 (AD 280)**	**P1 (AD 1300)**
Total DRE volume	0.67 - 0.88 km^3	0.16 km^3
Erupted mass	1.5 - 1.9 x 10^{12} kg	4 x 10^{11} kg
VEI	4	4
Magnitude	5.2	4.6
Maximum column height	22 - 26 km	19 - 22 km
Maximum PDC runout	7 - 11.5 km	4.5 - 8 km
Mass eruption rate	4 x 10^7 to 3.1 x 10^8 kg s^{-1}	1.6 x 10^7 to 9 x 10^7 kg s^{-1}
Maximum intensity	11.5	11
Duration	> 7h	> 5h
TGSD	D = 3.4 - 3.5	D = 3.2 - 3.3
Minimum exit velocity	180 - 200 m s^{-1}	150 - 165 m s^{-1}
Effective gas content	1.7 - 2.1 wt%	1.2 - 1.5 wt%

Table 2: Summary of the estimated eruptive parameters for the P2 AD 280 eruption (this study) and comparison with the P1 AD 1300 eruption (Carazzo et al., 2012).

Impact of the P2 eruption at the regional scale

The islands of Martinique and Dominica appear to have been occupied at the time of the P2 eruption of Mt. Pelée. Several sites with vestiges of the early Saladoid culture were found near rivers mostly along the northeastern coast of Martinique and in the south of Dominica. The poor river fishing and hunting resources in this region of Martinique suggest that these early inhabitants were farmers, as confirmed by the numerous pottery and grinding stones found in the excavations (Saunders 2005). A detailed comparison of the ceramic material

suggests that a small cultural group lived between Martinique and the south of Dominica, whereas the north of Dominica was occupied by a different group of farmers (Bérard 2007).

At many sites in Martinique, the archaeological artefacts are well-preserved under a layer of pumice fallout a few tens of centimeters thick, attributed to P2 (Revert 1948; Mattioni 1976; Rodriguez-Loubet 1994; Bérard et al. 2001). A fine layer of volcanic ash interpreted to be a blast deposit (P2i) is sometimes present between the archaeological level and the pumice fallout unit (P2A-C). A striking observation made at the Vivé site in Martinique is the presence of several ceramic vases standing on the living floor in their original context of use (Bérard et al. 2001). Additional observations made on cooking-pots and ceramic griddles led the archaeologists to conclude that an abrupt departure from the site had occurred. The P2 AD 280 eruption is famously known in Caribbean archaeology for having forced the first inhabitants of Martinique to flee to other islands such as Dominica or maybe even further north up to Guadeloupe where the first settlers arrived around AD 300.

The descendants of the survivors returned to Martinique around AD 400 (Rodriguez-Loubet 1994; Saunders 2005) where they mostly settled along the southern coast in a region with less fertile soils and far from potable water but at a safe distance from the volcano (Bérard 2007). Interestingly, a major explosive eruption occurred in the south of Dominica around AD 390 (Lindsay et al. 2005). This poorly documented event corresponds to an eruption of Morne Patates volcano that sealed several archaeological artefacts under a thick layer of ignimbrite deposit (Bérard 2007). There is no evidence that this eruption resulted in the return of settlers to Martinique but the concomitance of these events certainly raises the question of how the threat of volcanic eruptions led the first inhabitants of the Caribbean to adapt to their environment. The impact of the P2 eruption highlights the importance of assessing volcanic hazards in the Lesser Antilles at the scale of the Caribbean islands. The combination of field reconstruction and modeling of volcanic ash dispersion in the atmosphere should help in achieving this goal.

Conclusion

We have presented a new comprehensive field study of the P2 AD 280 eruption, and a detailed reconstruction of the mechanisms controlling the eruptive dynamics. After an initial opening phase characterized by the formation of a lateral blast to the northeast of the volcano (P2i), the eruption produced a 23-26 km-high stable column (P2A), which partially collapsed due to the increase of mass eruption rate (P2B). The column height then reached 22 km (P1C) before collapsing as a fountain-fed PDC (P2D). Our calculations show that P2 was a moderate Plinian eruption (VEI-4, M=5.2) evolving close to the plume/fountain transition. The total volume of tephra is estimated be larger than 0.67-0.88 km^3 DRE, and the mass eruption rate increased from ~7.5×10^7 to > 3.1×10^8 kg s^{-1} during a period of at least 7h.

The P2 eruption has a similar depositional sequence to that of the P1 AD 1300 eruption (Carazzo et al. 2012), but with slightly higher column heights, mass discharge rates, volume and duration. Both eruptions underwent a marginally stable evolution of the volcanic column whereby the flow behavior is highly sensitive to small variations of mass eruption rate, gas content, grain-size distribution of the pyroclasts and wind strength and direction. The recurrence of this phenomenon highlights the need to improve our understanding of this type of eruptive behavior with regard to assessing associated volcanic hazards and mitigate the risks at the local and regional scale around stratovolcanoes. The comparison of the model predictions of column collapse and field data from the four well-constrained eruptions of Taupo (≈186 CE), Vesuvius (79 CE) and Mt Pelée (P1 and P2) revealed a good agreement for only three eruptions. To better account for the conditions of transition at Vesuvius, which implied a higher fraction of large pyroclasts (D = 3.0), we suggest that thermal disequilibrium

should be incorporated in a new generation of models of volcanic plumes.

Acknowledgements

The authors warmly thank S. Self, and two anonymous reviewers, and the editor, J. Dufek for their constructive comments. We are very grateful to C. Martel and C. M. Vidal for fruitful discussions on magmatic water contents at Mt Pelée volcano. We warmly thank G. Delaviel-Anger, A. Fries and A. Michaud-Dubuy for their hard work in the field and for stimulating discussions. We thank J.E. Gardner, U. Kueppers, and D. Perugini for valuable assistance in the field and for their insightful comments on the P2 stratigraphy and grain-size distributions. We are grateful to our colleagues of the Institut National de Recherches Archéologiques Préventives, A. Jégouzo, A. Bolle, C. Martin, E. Moizan, C. Dunikowski, and O. Dayrens for sharing their field data. We are also indebted to the staff of the Mt Pelée volcanological observatory (OVSM) for field and administrative assistance. We also thank J.-P. Dumoulin, L. Beck, E. Delque-Kolic and C. Moreau (LMC14, CNRS UMS2572) who performed the ^{14}C dating. This work was partially funded by the Institut National des Sciences de l'Univers – Centre National de la Recherche Scientifique progamme CT3-ALEA, INSU-CNRS Artemis 2016 for ^{14}C dating, CASAVA (ANR contract ANR-09-ANR-RISK-002) and RAVEX (ANR contract ANR-16-CE03-0002). This is IPGP contribution No. XXXX.

References

Alibidirov M, Dingwell DB (1996) Magma fragmentation by rapid decompression. Nature 380:146-148

Arsandaux H (1929) Sur l'éruption actuelle de la Montagne Pelée. Bull Volcanol 6:25-32

Arsandaux H (1934) L'éruption de la Montagne Pelée en 1929. Rev. Scientifique 72:248-251

Bardintzeff JM, Miskovsky JC, Traineau H, Westercamp D (1989) The recent pumice eruptions of Mt. Pelée, Martinique. Part II: Grain-size studies and modelling the last Plinian phase P1. J Volcan Geotherm Res 38:35–48

Bérard B, Vernet G, Kieffer G, Raynal J-P (2001) Les eruptions volcaniques de la Montagne Pelée et le premier peuplement de la Martinique. In: *XIXème Congrès international d'Archéologie de la Caraïbe*, pp. 70-87

Bérard B (2007) The "South-Dominica" archaeological mission: the Soufrière site. In: *XXII Conference of the International Association of Caribbean Archaeology*, Jul. 2007, Kingston, Jamaica

Bernard M-L, Zamora M, Géraud Y, Boudon G (2007) Transport properties of pyroclastic rocks from Montagne Pelée volcano (Martinique, Lesser Antilles). J Geophys Res 112, B05205

Bonadonna C, Costa A (2012) Estimating the volume of tephra deposits: a new simple strategy. Geology 40(5):415-418

Bonadonna C, Costa A (2013) Plume height, volume, and classification of explosive volcanic

eruptions based on the Weibull function. Bull Volcanol 75:742-761

Bonadonna C, Houghton BF (2005) Total grain-size distribution and volume of tephra fall deposits. Bull Volcanol 67:441-456

Boudon, G (1993) *La montagne Pelée, Martinique: evolution volcanologique*, Societé géologique de France, Paris, France

Boudon G, Lajoie J (1989) The 1902 Pelean deposits in the Fort Cemetery of St. Pierre, Martinique: a model for the accumulation of turbulent nuées ardentes. J Volcan Geoth Res 38:113-130

Boudon G, Le Friant A, Villemant B, Viode J-P (2005) Martinique, in *Volcanic Hazard Atlas of The Lesser Antilles*, edited by Lindsay JM, Robertson REA, Shepherd JB, Ali S, pp. 127-146, Seismic Research Unit, The University of the West Indies, Trinidad and Tobago, W.I.

Boudon G, Villemant B, Le Friant A, Paterne M, Cortijo E (2013) Role of large flank-collapse events on magma evolution of volcanoes. Insights from the Lesser Antilles Arc. J Volcan Geotherm Res 263:224-237

Bourdier J-L, Gourgaud A, Vincent PM (1985) Magma mixing in a main stage of formation of Montagne Pelée: the Saint Vincent-type scoria flow sequence (Martinique, F.W.I.). J Volcan Geotherm Res 25-309-332

Bourdier JL, Boudon G, Gourgaud A (1989) Stratigraphy of the 1902 and 1929 nuée-ardente deposits, Mt. Pelée, Martinique. J Volcan Geotherm Res 38:77–96

Brunet M, Le Friant A, Boudon G, Lafuerza S, Talling P, Hornbach M, Ishizuka O, Lebas E, Guyard H and IODP Expedition 340 science Party (2016) Composition, geometry, and emplacement dynamics of a large volcanic island landslide offshore Martinique: From volcano flank-collapse to seafloor sediment failure? Geochemistry, Geophysics, Geosystems, 17(3), 699-724

Bursik MI, Woods AW (1996) The dynamics and thermodynamics of large ash flows. Bull Volcanol 58:175– 193

Calder ES, Cole PD, Dade WB, Druitt TH, Hoblitt RP, Huppert HE, Ritchie L, Sparks RSJ, Young SR (1999) Mobility of pyroclastic flows and surges at the Soufriere Hills Volcano, Montserrat. Geophys Res Lett 26:537–540

Carazzo G, Kaminski E, Tait S (2008a) On the dynamics of volcanic columns: A comparison of field data with a new model of negatively buoyant jets. J Volcanol Geoth Res 178:94-103. doi:10.1016/j.jvolgeores.2008.01.002

Carazzo G, Kaminski E, Tait S (2008b) On the rise of turbulent plumes: quantitative effects of variable entrainment for submarine hydrothermal vents, terrestrial and extra terrestrial explosive volcanism. J Geophys Res 113:B09201. doi:10.1029/2007JB00548

Carazzo G, Tait S, Kaminski E, Gardner JE (2012) The recent Plinian explosive activity of Mt. Pelée volcano (Lesser Antilles): The P1 AD 1300 eruption, Bull Volcanol 74:2187-2203

Carey S, Sigurdsson H (1987) Temporal variations in column height and magma discharge rate during the 79 A.D. eruption of Vesuvius. Geol Soc Am Bull 99:303–314

Carey S, Sigurdsson H (1989) The intensity of Plinian eruptions. Bull Volcanol 51:28–40

Carey S, Sparks RSJ (1986) Quantitative models of the fallout and dispersal of tephra from volcanic eruption columns. Bull Volcanol 48:109–125

Carey S, Sigurdsson H, Gardner JE, Criswell W (1990) Variations in column height and magma discharge during the May 18, 1980 eruption of Mount St. Helens. J Volcanol Geoth Res43:99-112

Costa A, Suzuki YJ, Cerminara M, Devenish BJ, Esposito Ongaro T, Herzog M, Van Eaton AR, Denby LC, Bursik M, de' Michieli Vitturi M, Engwell S, Barsotti S, Folch A, Macedonio G, Girault F, Carazzo G, Tait S, Kaminski E, Mastin LG, Woodhouse MJ, Phillips JC, Hogg AJ, Degruyter W, Bonadonna C (2016) Results of the eruptive column model inter-comparison study. J Volcanol Geotherm Res 326: 2-25

Dade WB, Huppert HE (1998) Long runout rockfalls. Geology 26:803–806

Daggit ML, Mather TA, Pyle DM, Page S (2014) AshCalc – a new tool for the comparison of the exponential, power-law and Weibull models of tephra deposition. J Appl Volcanol 3:7

Davidson J, Wilson M (2012) Differentiation and source processes at Mt Pelée and the Quill; Active volcanoes in the Lesser Antilles arc. J Petrol 52(7-8):1493-1531

Doyle EE, Hogg AJ, Mader HM, Sparks RSJ (2010) A two-layer model for the evolution and propagation of dense and dilute regions of pyroclastic currents. J Volcanol Geotherm Res 190:365–378

Dupuy C, Dostal J, Traineau H (1985) Geochemistry of volcanic rocks from Mt. Pelée, Martinique. J Volcanol Geotherm Res 26:147–165

Fierstein J, Nathenson M (1992) Another look at the calculation of fallout tephra volumes. Bull Volcanol 54(2):156– 167

Fisher RV, Smith AL, Roobol MJ (1980) Destruction of St. Pierre, Martinique, by ash-cloud surges, May 8 and 20, 1902, Geology 8:472-476

Genevey A, Gallet Y, Boudon G (2002) Secular variation study from non-welded pyroclastic deposits from Montagne Pelée volcano, Martinique (West Indies). Earth Planet Sci Lett 201:369-382

Germa A, Quidelleur X, Labanieh S, Chauvel C, Lahitte P (2011) The volcanic evolution of Martinique Island: insights from K-Ar dating into the Lesser Antilles arc migration since the Oligocene, J Volcan Geotherm Res 208:122-135

Germa A, Lahitte P, Quidelleur X (2015) Construction and destruction of Mont Pelée volcano: volumes and rates constrained from a geomorphological model of evolution, J Geophys Res Earth Surf 120:1206-1226

Girault F, Carazzo G, Tait S, Ferrucci F, Kaminski E (2014) The effect of total grain-size distribution on the dynamics of turbulent volcanic plumes, Earth Plan Sci Lett 394:124-134

Girault F, Carazzo G, Tait S, Kaminski E (2016) Combined effects of total grain-size distribution and crosswind on the rise of eruptive volcanic columns, J Volcanol Geotherm Res, in press

Hartmann WK (1969) Terrestrial, lunar and interplanetary rock fragmentation. Icarus 10:201-213

Kaminski E, Jaupart C (1998) The size distribution of pyroclasts and the fragmentation sequence in explosive volcanic eruptions. J Geophys Res 103:29,759–29,779

Komorowski JC, Legendre Y, Caron B, Boudon G (2008) Reconstruction and analysis of sub-plinian tephra dispersal during the 1530 AD Soufriere (Guadeloupe) eruption: implications for scenario definition and hazards assessment. J Volcanol Geotherm Res 178:491–515

Koyaguchi T, Ohno M (2001) Reconstruction of eruption column dynamics on the basis of grain size of tephra fall deposits 1. Methods. J Geophys Res 106:6499-6512

Koyaguchi T, Suzuki Y J, Kozono T (2010) Effects of the crater on eruption column dynamics. J. Geophys. Res. 115, B07205

Kueppers U, Perugini D. Dingwell DB (2006) "Explosive energy" during volcanic eruptions from fractal analysis of pyroclasts. Earth Planet Sci Lett 248:800-807

Lacroix A (1904) La Montagne Pelée et ses éruptions. Masson, Paris

Lajoie J, Boudon G, Bourdier J-L (1989) Depositional mechanics of the 1902 pyroclastic nuée-ardente deposits of Mt. Pelée, Martinique. J Volcanol Geotherm Res 38:131-142

Le Friant A, Boudon G, Deplus C, Villemant B (2003) Large-scale flank collapse events during the activity of Montagne Pelée, Martinique, Lesser Antilles, J Geophys Res 108(B1)

Lindsay JM, Smith AL, Roobol MJ, Stasiuk MV (2005) Dominica, in *Volcanic Hazard Atlas of The Lesser Antilles*, edited by Lindsay JM, Robertson REA, Shepherd JB, Ali S, pp. 1-48, Seismic Research Unit, The University of the West Indies, Trinidad and Tobago, W.I.

Martel C (2012) Eruption dynamics inferred from microlite crystallization experiments: Application to Plinian and dome-forming eruptions of Mt Pelée (Martinique, Lesser Antilles). J Petrol 53(4):699-725

Martel C, Poussineau S (2007) Diversity of eruptive styles inferred from the microlites of Mt. Pelée andesite (Martinique, Lesser Antilles). J Volcanol Geotherm Res 166:233– 254

Martel C, Pichavant M, Bourdier J-L, Traineau H, Holtz F, Scaillet B (1998) Magma storage conditions and control of eruption regime in silicic volcanoes: experimental evidence from Mt. Pelée. Earth Planet Sci Lett 156:89–99

Martel C, Bourdier JL, Pichavant M, Traineau H (2000) Textures, water content and

degassing of silicic andesites from recent Plinian and dome-forming eruptions at Mt. Pelée volcano (Martinique, Lesser Antilles arc). J Volcanol Geotherm Res 96:191–206

Mattioni M (1976) Les grandes familles de formes du saladoïde insulaire du site de Vivé à la Martinique. *Proceedings of the 6th International congress for the study of the pre-Columbian cultures of the Lesser Antilles*, p. 11-33

Michaud-Dubuy A, Carazzo G, Kaminski E, Girault F (2018) A revisit of the role of gas entrapment on the stability conditions of explosive volcanic columns. J. Volcanol Geotherm Res 357: 349-361.

Neri A, Dobran F (1994) Influence of eruption parameters on the thermofluid dynamics of collapsing volcanic columns. J Geophys Res 99(B6):11,833-11,857

Newhall CG, Self S (1982) The volcanic explosivity index (VEI): an estimate of explosive magnitude for historical volcanism. J Geophys Res 87:1231–1238

Perret FA (1931a) Le nouveau dôme de la Montagne Pelée. Compt Rend Acad Sci, Paris, 193:1342-1344

Perret FA (1931b) Le dôme recent de la Montagne Pelée. Compt Rend Acad Sci, Paris, 193:1439-1442

Perret FA (1935) *The eruption of Mount Pelée 1929-1932*. Carnegie Institution of Washington, 125 p.

Perrey A (1853) Note sur les tremblements de terre en 1851. Memoire Académie Sciences, Arts et Belles-Lettres, Dijon 2:1-65

Pyle DM (1989) The thickness, volume and grainsize of tephra fall deposits. Bull Volcanol 51:1–15

Pyle DM (1995) Mass and energy budgets of explosive volcanic eruptions. Geophys Res Lett 22:563–566

Pyle DM (2000) Sizes of volcanic eruptions. In: Sigurdsson H, Houghton B, Reimer H, Stiw J, McNutt S (eds) Encyclopedia of volcanoes. Academic, San Diego, pp 263-269

Quantin P, Balesdent J, Bouleau A, Delaune, Feller C (1991) Premiers stades d'altération de ponces volaniques en climat tropical humide (Montagne Pelée, Martinique). Geoderma 50:125-148

Revert E (1931) La Montagne Pelée et ses dernières éruptions. Ann. Geogr. 40:275-291

Revert E (1948) Fouilles et sites précolombiens de la Martinique. Etudes rhodaniennes 23:172-176

Rodriguez-Loubet F. (1994) Les Antilles, un des derniers peuplements précolombiens de l'Amérique. Bull Soc Préhisto Fr 91:324-332

Romer M (1931) La dernière eruption de la Montagne Pelée. Bull Volcanol 8:89-116

Romer M (1934) L'éruption de la Montagne Pelée (Martinique) de 1929 à 1933. Annales de Physique du Globe de la France d'Outre-Mer 5:129-147

Roobol MJ, Smith AL (1976) Mount Pelée, Martinique: a pattern of alternating eruptive styles. Geology 4:521–524

Roobol MJ, Smith AL (1980) Pumice eruptions of the Lesser Antilles. Bull Volcanol 43:277–286

Roobol MJ, Smith AL (2004) *Volcanology of Saba and St. Eustatius*, Northern Lesser Antilles. Koninklijke nederlandse Akademie van wetenschappen

Ruzié L, Moreira M (2010) Magma degassing process during plinian eruptions. J Volcanol Geotherm Res 192:142–150

Saunders NJ (2005) *The peoples of the Caribbean: An encyclopedia of Caribbean archaeology and traditional culture*, Santa Barbara, CA: ABC

Sigurdsson H, Carey S (1989) Plinian and co-ignimbrite tephra fall from the 1815 eruption of Tambora volcano. Bull Volcanol 51:243-270

Sigurdsson H, Carey S, Fisher RV (1984) The 1982 eruptions of El Chichon volcano, Mexico: Stratigraphy of pyroclastic deposits. J Volcanol Geotherm Res 23:11-37

Suzuki YJ, Koyaguchi T, Ogawa M, Hachisu I (2005) A numerical study of turbulent mixing in eruption clouds using a three-dimensional fluid dynamics model. J Geophys Res 110, B08201

Traineau H, Westercamp D, Coulon C (1983) Mélanges magmatiques à la Montagne Pelée (Martinique). Origine des éruptions de type Saint-Vincent, Bull Volcanol 46(3):243-269

Traineau H, Westercamp D, Bardintzeff JM, Miskovsky JC (1989) The recent pumice eruptions of Mt. Pelée volcano, Martinique. Part I: Depositional sequences, description of pumiceous deposits. J Volcanol Geotherm Res 38:17–33

Turcotte DL (1986) Fractals and fragmentation. J Geophys Res 91:1921-1926

Valentine GA, Wohletz KH (1989) Numerical models of Plinian eruption columns and pyroclastic flows. J Geophys Res 94-1867-1887

Vidal CM, Komorowski J-C, Métrich N, Pratomo I, Kartadinata N, Prambada O, Michel A, Carazzo G, Lavigne F, Rodysill J, Fontijn K, Surono (2015) Dynamics of the major Plinian eruption of Samala in 1257 A.D. (Lombok, Indonesia). Bull Volcanol 77:73. doi: 10.1007/s00445-015-0960-9

Villemant B, Boudon G (1998) Transition from dome-forming to plinian eruptive styles controlled by H_20 and Cl degassing. Nature 392:65–69

Villemant B, Boudon G (1999) H_20 and halogen (F, Cl, Br) behaviour during shallow magma degassing processes. Earth Planet Sci Lett 168:271–286

Villemant B, Boudon G, Komorowski JC (1996) U-series disequilibrium in arc magmas induced by water-magma interaction. Earth Planet Sci Lett 140:259–267

Vincent PM, Bourdier J-L, Boudon G (1989) The primitive volcano of Mount Pelée: its construction and partial destruction by flank collapse. J Volcanol Geotherm Res 38:1-15

Walker GPL (1980) The Taupo pumice: product of the most powerful known (ultraplinian) eruption. J Volcanol Geoth Res 8:69-94

Westercamp D, Traineau H (1983) The past 5,000 years of volcanic activity at Mt. Pelée Martinique (F.W.I.): Implications for assessment of volcanic hazards. J Volcanol Geotherm Res 17:159–185

Wilson L (1976) Explosive volcanic eruptions-III. Plinian eruption columns. Geophys J R Astrom Soc 45:543–556

Wilson L, Sparks RSJ, Walker GPL (1980) Explosive volcanic eruptions-IV. The control of magma properties and conduit geometry on eruption column behaviour. Geophys J R Astrom Soc 63:117–148

Woods AW, Bursik MI (1991) Particle fallout, thermal disequilibrium and volcanic plumes. Bull Volcanol 53: 559-570

Wright JV, Smith AL, Roobol MJ, Mattioli GS, Fryxell JE (2016) Distal ash hurricane (pyroclastic density current) deposits from a ca. 2000 yr B.P. Plinian-style eruption of Mount Pelée, Martinique: Distribution, grain-size characteristics, and implications for future hazards, Geol Soc Am Bull 128:777-791